The Journal of Chemical Physics

RESEARCH ARTICLE | OCTOBER 01 2024

X-ray photoelectron and NEXAFS spectroscopy of thionated uracils in the gas phase

Dennis Mayer ; Max Handrich ; David Picconi ; Fabiano Lever ; Lisa Mehner ; Marta L. Murillo-Sanchez ; Constantin Walz ; Evgenii Titov ; John Bozek ; Peter Saalfrank ; Markus Gühr

J. Chem. Phys. 161, 134301 (2024)
https://doi.org/10.1063/5.0226983

AIP Publishing

The Journal of Chemical Physics ARTICLE pubs.aip.org/aip/jcp

X-ray photoelectron and NEXAFS spectroscopy of thionated uracils in the gas phase

Cite as: J. Chem. Phys. 161, 134301 (2024); doi: 10.1063/5.0226983
Submitted: 5 July 2024 • Accepted: 13 September 2024 •
Published Online: 1 October 2024

Dennis Mayer,[1,a)] Max Handrich,[2] David Picconi,[3] Fabiano Lever,[1] Lisa Mehner,[4] Marta L. Murillo-Sanchez,[5] Constantin Walz,[4] Evgenii Titov,[2] John Bozek,[6] Peter Saalfrank,[2,4] and Markus Gühr[1,7]

AFFILIATIONS

[1] Deutsches Elektronen-Synchrotron DESY, Notkestr. 85, 22607 Hamburg, Germany
[2] Institut für Chemie, Universität Potsdam, Karl-Liebknecht-Str. 24/25, 14476 Potsdam, Germany
[3] Institut für Theoretische Chemie und Computerchemie, Heinrich-Heine-Universität Düsseldorf, Universitätsstr. 1, 40225 Düsseldorf, Germany
[4] Institut für Physik und Astronomie, Universität Potsdam, Karl-Liebknecht-Str. 24/25, 14476 Potsdam, Germany
[5] Max-Planck-Institut für Kernphysik, Saupfercheckweg 1, 69117 Heidelberg, Germany
[6] Synchrotron SOLEIL, L'Orme de Merisiers, Départementale 128, 91190 Saint-Aubin, France
[7] Institut für Physikalische Chemie, Universität Hamburg, Grindelallee 117, 20146 Hamburg, Germany

[a)] **Author to whom correspondence should be addressed:** dennis.mayer@desy.de

ABSTRACT

We present a comprehensive, combined experimental and theoretical study of the core-level photoelectron and near-edge x-ray absorption fine structure (NEXAFS) spectra of 2-thiouracil, 4-thiouracil, and 2,4-dithiouracil at the oxygen 1s, nitrogen 1s, carbon 1s, and the sulfur 2s and 2p edges. X-ray photoelectron spectra were calculated using equation-of-motion coupled-cluster theory (EOM-CCSD), and NEXAFS spectra were calculated using algebraic diagrammatic construction and EOM-CCSD. For the main peaks at O and N 1s as well as the S 2s edge, we find a single photoline. The S 2p spectra show a spin–orbit splitting of 1.2 eV with an asymmetric vibrational line shape. We also resolve the correlation satellites of these photolines. For the carbon 1s photoelectrons, we observe a splitting on the eV scale, which we can unanimously attribute to specific sites. In the NEXAFS spectra, we see very isolated pre-edge features at the oxygen 1s edge; the nitrogen edge, however, is very complex, in contrast to the XPS findings. The C 1s edge NEXAFS spectrum shows site-specific splitting. The sulfur 2s and 2p spectra are dominated by two strong pre-edge transitions. The S 2p spectra show again the spin–orbit splitting of 1.2 eV.

INTRODUCTION

Thiouracils are analogs of the naturally occurring nucleobase uracil, obtained by replacing one or both oxygen atoms with sulfur.[1] Thionucleobases, in general, have a long-standing history in medical treatment and research being used in cancer therapy, immunosuppression, hyperthyroidism treatment, or UV cross-linking.[2,3] The substitution of oxygen by sulfur leads to significant photophysical and photochemical changes in the molecules. These include a strong red shift of the UV absorption and a fast relaxation into triplet states.[2,3] The latter contrasts the photodynamical behavior of their canonical counterparts, which relax quickly into their ground state after photoexcitation, a feature that contributes to their photostability.[4]

The different photophysics of thionated nucleobases has drawn attention in recent years, and many studies have been conducted to develop a good understanding of the relaxation mechanisms of these molecules (see Refs. 2 and 3 and references therein). Among these, thiouracils (see Scheme 1) are the most thoroughly studied samples right now. The literature contains a variety of spectroscopic experiments performed with visible and UV light for both static and time-resolved spectroscopy;[5–21] hence, the valence electronic ground-state structure is well established.[9,16,18,22–26] With the availability of x-ray free-electron lasers (FELs), the pool of experimental studies on

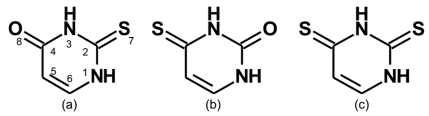

SCHEME 1. Structural formula of (a) 2-thiouracil, (b) 4-thiouracil, and (c) 2,4-dithiouracil. The atom numbering in (a) is used for all three molecules.

nucleobases has been recently enhanced by means of time-resolved x-ray photoelectron, Auger–Meitner, and x-ray absorption spectroscopies, shifting the focus from probing the dynamics via valence electron transitions (in transient absorption or valence photoelectron spectroscopy) toward highly localized inner-shell electrons.[27–31] These experiments utilize the site- and element selectivity of x rays in order to obtain a more direct insight into charge flows and geometrical changes that are directly correlated to the transient electronic states.

However, the literature on the core-level spectroscopy of thiouracil is still sparse. To our knowledge, only one study of synchrotron measurements has been published thus far.[32] These measurements have been conducted at the Elettra synchrotron in Trieste and cover only the x-ray photoelectron spectroscopy (XPS) of 2-thiouracil (2-tUra). Measurements performed by the authors at the free-electron laser FLASH also include parts of the static x-ray spectroscopy of 2-tUra,[27,28,33] but these measurements are strongly limited in spectral resolution due to the large bandwidth of the x-ray pulses used for these experiments.[34] This means, for example, that the measurement of the S 2p photoline appears as a single feature in FEL experiments due to the broad spectral width of the pulses, whereas synchrotron measurements show spin–orbit splitting of 1.2 eV.[32,34] Furthermore, 4-thiouracil (4-tUra) and 2,4-dithiouracil (2,4-dtUra) have not been studied with x-ray spectroscopic methods so far, to the best of our knowledge. Only a computational study on the time-resolved x-ray absorption spectra of 4-tUra has recently been published.[35] Here, we report a combined experimental and theoretical study on the x-ray photoelectron spectroscopy (XPS) and near edge x-ray absorption fine structure (NEXAFS) spectra of the three thionated nucleobases 2-tUra, 4-tUra, and 2,4-dtUra to fill the gap in spectroscopic data on the three thiouracils. Spectra are reported for the sulfur L edges and the carbon, nitrogen, and oxygen K edges.

METHODS

Experiment

The experiments were performed at the PLEIADES beamline of the synchrotron SOLEIL.[36] Thiouracil was evaporated at temperatures of ~120 °C using a heatable cartridge inside the main vacuum chamber. At these temperatures, the vapor pressure of thiouracils is in the order of $1 \cdot 10^{-4}$ mbar.[37] The pressure in the main chamber was around $1 \cdot 10^{-7}$ mbar during the experiments. The pressure in the gas cell could not be measured but had to be somewhere between the vapor pressure of the sample and the main chamber pressure. The x-ray beam was produced by an Apple II HU 80 permanent magnet undulator, and the exact photon energy was selected using a 600 lines/mm grating. The beam could enter and exit the cartridge via pinholes. The focal size of the beam inside the gas cell is ca. 100 μm wide in the horizontal dimension. In the vertical dimension, the beam is an image of the monochromator exit slit and, thus, ca. 100 μm. The flux of the beam depends on the monochromator slit size and photon energy used. For the used photon energies, the flux is typically in the order of $5 \cdot 10^{12}$ photons/s. Electrons generated by the interaction of the x-ray beam with the sample vapor could exit the cartridge perpendicular to the beam path via a slit that faced the entrance of a hemispherical electron kinetic energy analyzer (Scienta R4000). Photoelectron spectra were taken at the sulfur L edges and carbon, nitrogen, and oxygen K edges using photon energies of 250 eV (S 2p), 330 eV (S 2s), 382 eV (C 1s), 495 eV (N 1s), and 628 eV (O 1s) with the overall estimated resolutions of 100, 200, 140, 300, and 470 meV, respectively. A complete set of the parameters of the monochromator and the hemispherical analyzer can be found in Table VIII in the Appendix. The NEXAFS spectra for the same edges were obtained by measuring and integrating resonant Auger–Meitner (or Coster–Kronig) electron spectra with the hemispherical analyzer while scanning the photon energy around the respective ionization edge in steps of 0.25 eV. The monochromator exit slit size was chosen for each edge so that it matches the 0.25 eV step size. The numbers for the energy resolution for each molecule and edge can be found in Table IX in the Appendix.

Computational details

The vertical core ionization and excitation energies for 2-tUra, 4-tUra, and 2,4-dtUra were calculated at the ground-state minima of the molecules. These structures were obtained by geometry optimizations performed using coupled-cluster theory with singles and doubles (CCSD) and the 6-31++G** basis set.[38,39] Geometry optimizations were performed using the program Q-Chem 4.4.[40] The minima were found to be planar for all the thionucleobases, and their stability was checked by frequency calculations at the same level of theory.

XPS spectra

The core ionization energies at the different edges were computed using the equation-of-motion coupled-cluster theory for ionization potential, adopting the core–valence separation scheme with frozen core to make the calculations numerically stable (fc-CVS-EOM-IP-CCSD).[41] Following Ref. 42, the 6-311+G(3df) basis set was used, with uncontracted core functions on the carbon, nitrogen, oxygen, or sulfur atoms, depending on the edge of interest. Only the energies of the dominant ionization channels, with the valence configuration unchanged, were computed. The ionization intensity was approximated using Dyson norms. For the S 2p edge, the XPS peaks are split due to core-hole spin–orbit coupling. Therefore, the full spin–orbit coupling matrix was evaluated using a procedure based on the Wigner–Eckart theorem,[43] and the full electronic Hamiltonian was then diagonalized to get the relativistically corrected ionization potentials. The calculations were performed using the Q-Chem 5.3 package.[44]

The computed XPS peaks were further shifted to facilitate the comparison with the experimental spectra. Each shift is edge-specific and given by the average of the best match for each molecule at the respective edge. The extent of each shift is typically dependent on the chosen basis set, and it is difficult to find a basis that delivers the same shift for all edges.[40] Furthermore, edge-specific scalar

relativistic effects, not accounted for in the present simulations, might lead to an additional shift.[41]

NEXAFS spectra

The core absorption energies at the C 1s, N 1s, O 1s, and S 2s edges were computed using the extended variant of the second-order algebraic diagrammatic construction theory with the 6-311++G** basis set[45,46] and adopting the core–valence separation [CVS-ADC(2)-x].[47] For these calculations, the program Q-Chem 4.4 was used. The ADC(2)-x scheme has been shown to improve the treatment of doubly excited states ("shake-up" transitions), which are typically predicted too high in energy by the strict "ADC(2)-s" variant.[48] For the S 2p edge, the NEXAFS peaks are split due to the core-hole spin–orbit coupling (SOC). Because the calculation of the SOC at the ADC(2) level is not available in Q-Chem, the S 2p NEXAFS energies and intensities were computed using the equation-of-motion formalism of coupled-cluster theory (EOM-CCSD) with core–valence separation and the 6-311+G(3df) basis with uncontracted core on the sulfur atoms, as detailed in Ref. 42. Spin–orbit coupling was evaluated by augmenting the Hamiltonian with the Breit–Pauli spin–orbit coupling operator, adopting a mean field approximation for the two-electron part, as described in Ref. 49. Using Q-Chem 5.3 for these calculations, the augmented Hamiltonian was diagonalized in the basis of non-relativistic wave functions to obtain spin–orbit-corrected core-excited states. The assignment of the most intense NEXAFS transitions is detailed in the Appendix.

RESULTS AND DISCUSSION

X-ray photoelectron spectra

Oxygen 1s

We begin with the presentation and discussion of the photoelectron spectra of the three thiouracils. In Fig. 1(a), the O 1s XPS spectra of 2-tUra and 4-tUra are shown. We find a binding energy of 537.6 eV for 2-tUra, which agrees with the current literature value,[32] and 537.5 eV for 4-tUra. The width of the main photolines is 400 meV for 2-tUra and 550 meV for 4-tUra, which are broader than the natural linewidth for oxygen (~170 meV)[50] but in the order for the chosen resolution for this edge. A slight asymmetry in the spectra might originate from vibrational broadening. The results of the CCSD calculations are shown as gray sticks in Fig. 1(a) and are summarized in Table I. The results were shifted by −1.53 eV to match the experimental values and give a binding energy of 537.52 eV for 2-tUra and 537.58 eV for 4-tUra, respectively, after shift.

At higher binding energies, smaller peaks are observed in both experimental O 1s spectra. For 2-tUra, there is a maximum at 543 eV, and for 4-tUra, there are two small maxima at 540 and 543.5 eV. The satellite peak for 2-tUra has been observed in a previous study and was attributed to a shake-up process.[32] The second satellite at 543.5 eV in the 4-tUra spectrum falls also into the range of possible valence excitations, and it is hence reasonable to assume that this peak can be attributed to a shake-up process.[9] The first peak, however, is only 2.5 eV away from the main photoline, which

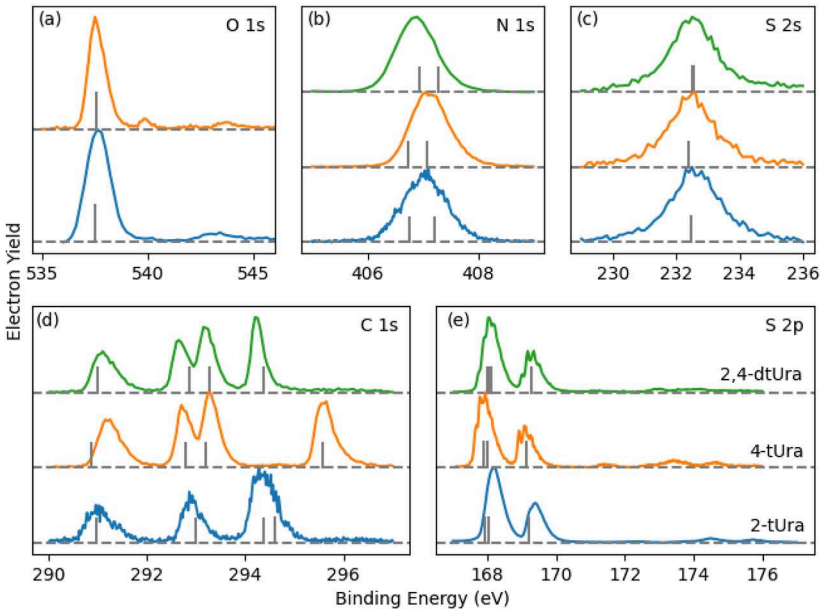

FIG. 1. X-ray photoelectron spectra of thionated uracils at the O, N, and C K edges (a), (b), and (d) and S L edges (c) and (e). The solid lines are experimental data. The sticks indicate the calculated binding energies for the core-level electrons shifted by −1.53, −0.90, −0.81, −0.46, and +0.18 eV for O 1s, N 1s, C 1s, S 2s, and S 2p, respectively. Each shift is the average of the best match for each molecule at the respective edge. The order/color code of the molecules stated in (e) applies for all panels (blue—2-tUra, orange—4-tUra, and green—2,4-dtUra).

TABLE I. Summary of the experimental and calculated binding energies of 2-thiouracil, 4-thiouracil, and 2,4-dithiouracil. Values are given in eV.

	2-Thiouracil		4-Thiouracil		2,4-Dithiouracil		
Core-level	Theory[a]	Exp.[b]	Theory[a]	Exp.[b]	Theory[a]	Exp.[b]	Assign.
S $2p_{3/2}$	167.95 168.05	168.2	167.91 168.00	167.9	168.02 168.12 168.04 168.13	168.0	S_7 S_8
S $2p_{1/2}$	169.19	169.4	169.15	169.1	169.27 169.28	169.2	S_7 S_8
S 2s	232.91	232.5	232.86	232.6	232.98 232.99	232.5	S_7 S_8
C 1s	290.96 292.98	291.0 292.9	290.85 292.79	291.2 292.7	291.00 292.87	291.2 292.7	C_5 C_6
	294.36 294.61	294.3	293.20 295.58	293.3 295.6	293.27 294.37	293.2 294.3	C_2[c]/C_4[d] C_4[c]/C_2[d]
N 1s	406.75 407.22	407.0	406.73 407.08	407.1	406.93 407.27	406.9	N_3 N_1
O 1s	537.52	537.6	537.58	537.5			O_8[c]/O_7[d]

[a]The values have been shifted by −1.53, −0.90, −0.81, −0.46, and +0.18 eV for O 1s, N 1s, C 1s, S 2s, and S 2p edges, respectively. Each shift is the average of the best match for each molecule at the respective edge.
[b]Values represent centers of (multi-)Gaussian fit of the experimental spectra.
[c]Applies for 2-thiouracil.
[d]Applies for 4-thiouracil and 2,4-dithiouracil.

is outside the expected range for valence excitations of the molecule. Referring to the literature, a small water contamination could lead to a feature at 540 eV.[51]

Nitrogen 1s

The N 1s photoelectron spectra for the three molecules are shown in Fig. 1(b). Only one feature is observed for all molecules. The binding energy is measured to be 407.0 eV for 2-tUra in agreement with the literature,[32] 407.1 eV for 4-tUra and 406.9 eV for 2,4-dtUra. The width of the peaks is 400, 350, and 360 meV for 2-tUra, 4-tUra, and 2,4-dtUra, respectively, and thus broader than the expected lifetime broadening of 130 meV[50] but again comparable to the chosen resolution for this edge. The calculations [gray sticks in Fig. 1(b)] exhibit two well-separated features, one for each N atom, at 406.75 and 407.22 eV for 2-tUra, 406.73 and 407.08 eV for 4-tUra, and 406.92 and 407.27 eV for 2,4-dtUra. All values have been shifted by −0.90 eV to match the experimental ones. In all three thiouracils, the 1s electron of the N_3 atom is slightly weaker bound than that of the N_1 atom. The difference between the nitrogen atoms is slightly larger in 2-tUra (~0.5 eV) than in the other two thiouracils (~0.35 eV). The broader split in 2-tUra might be the reason for the slightly broader peak in the experiment. Considering the significant theoretical splitting between the two nitrogen atoms and the capabilities of modern synchrotron beamlines, it can be reasonable to investigate N 1s edge with a better resolution in the future again to see whether it is possible to identify the individual contributions of the nitrogen atoms.

Carbon 1s

The C 1s spectra are shown in Fig. 1(d). 2-Thiouracil shows three peaks at 291, 292.9, and 294.3 eV, carrying about double the strength compared to the other peaks. The binding energy and strength agree with previous results.[32] Four peaks are visible for the other two molecules. In the case of 4-tUra, these are located at 291.2, 292.7, 293.3, and 295.6 eV. For 2,4-dtUra, they are at 291.2, 292.7, 293.2, and 294.3 eV. The theoretical results agree fairly well with the experiment. For 2-tUra, the CCSD calculations (gray sticks) give 290.96, 292.98, 294.36, and 294.61 eV. Apparently, the experimental peak with the largest binding energy appears to be a combination of two close lying ionization channels. However, the splitting is not resolved experimentally. The reason for this might be a combination of a slightly to coarse resolution of the experimental system as the lifetime broadening can be expected to be on the order of 100 meV[50] and, additional vibrational broadening or post-collision interaction (PCI) effects considering the asymmetry of the maxima in the spectrum. With the given photon energy of 382 eV, however,

the photoelectrons are too fast (~100 eV kinetic energy) to be significantly affected by the Auger electrons (~250 eV) and, thus, PCI should be negligible. For 4-tUra, the calculations give again four separated features at 290.85, 292.79, 293.20, and 295.58 eV. Apart from the maximum with the lowest binding energy, the energies agree well with the experiment. The four peaks for 2,4-dtUra are at 291.00, 292.87, 293.27, and 294.37 eV. In all three cases, the given values have been shifted by −0.81 eV to match the experiment better.

The assignment to specific atoms follows from the simulations. However, due to its educational value, we also estimate this on a qualitative level.[52,53] The pyrimidine ring of the thiouracils exhibits four carbon atoms (see Scheme 1). All the carbons have a different chemical environment and face atoms with different electronegativities than carbon (e.g., the Pauling electronegativity values of the involved atoms are C: 2.55, N: 3.04, O: 3.44, and S: 2.58).[54] By evaluating the surrounding of the C atoms, one can make the following attribution. The peak at the lowest binding energy in all three molecules belongs to the C_5 atom as it is only surrounded by other C atoms with the same electronegativity, thus leaving bonds unpolarized. The second lowest peak belongs to the C_6 atom as the neighboring N atom slightly draws charge away from the C because of its higher electronegativity. The third peak in 4-tUra and 2,4-dtUra can be attributed to the C_4 atom because sulfur and nitrogen are both more electronegative than carbon. Finally, the fourth peak in the two molecules belongs to the C_2 atom, which is surrounded by two N atoms and either an O or an S atom, all of which have a higher electronegativity than C. The same four-peak structure and assignment can also be found in the canonical counterpart uracil.[55] For 2-tUra, the third peak is a combination of C_4 and C_2 as oxygen has a much stronger impact on the valence charge distribution due to its significantly higher electronegativity. For this peak, the CCSD calculation adds to this more heuristic assignment as it suggests that C_4 is slightly stronger bound than C_2, but the difference is too small to be resolved in the experiment.

Sulfur 2s

We continue with the sulfur L edges. The S 2s spectra are shown in Fig. 1(c). All three molecules show a single broad feature, which is located at 232.5, 232.6, and 232.5 eV for 2-tUra, 4-tUra, and 2,4-dtUra, respectively. The spectra have a full width at half maximum of about 1.6 eV, which is comparable to the natural linewidth of the S 2s level in other sulfur containing molecules.[56] The CCSD calculations (gray sticks) give 232.52, 232.48, and 232.61 eV for the three molecules after shifting by −0.46 eV to match the experiment.

Sulfur 2p

Figure 1(e) shows the x-ray photoelectron spectra at the S 2p edge. We observe a spin–orbit (SO) split photoline in all three molecules. The value of the SO-splitting is in all three cases 1.2 eV. For 2-tUra, the photolines are located at 168.2 eV ($2p_{3/2}$) and 169.4 eV ($2p_{1/2}$) in agreement with the previous literature.[32] With about −0.3 eV, the photoline in 4-tUra is slightly shifted against that of 2-tUra giving values at 167.9 and 169.1 eV. The shift is slightly less in 2,4-dtUra, and the two S 2p peaks are found at 168.0 and 169.2 eV. The width of the lines is about 230 meV in all molecules, which is broader than the expected natural linewidth of ~100 meV.[50] The asymmetry of the maxima indicates that vibrational excitation or PCI further broaden the spectrum. Post-collision interaction, however, should be negligible due to very similar excess energies of the photoelectrons (~80 eV) and Auger electrons (100–140 eV).

Furthermore, we observe for all three molecules much smaller peaks at higher binding energies, which we attribute to shake-up satellites during the ionization process.[57,58] In the case of 2-tUra, we identify an enhanced signal at 174.5 and 175.7 eV, which is about 10 times weaker than the actual photoline. These satellites have also been observed in a previous FEL study, however, without the 1.2 eV SO-splitting due to a lack of resolution.[27] In 4-tUra, three somewhat distinct peaks are observed at 171.4, 173.4, and 174.6 eV, and in 2,4-dtUra, additional maxima are located at 172.9 and 174.0 eV. It is not excluded that more satellites can be observed at higher binding energy values, but a thorough investigation of these features was beyond the scope of the study.

The CCSD calculations (gray sticks) for the S 2p levels do not account for shake-up processes; hence, the satellites are not reproduced. However, they include the SO-coupling and, after shifting by +0.175 eV, they result in a good match with the experiment. Note that the peak is contributed by two transitions of slightly different ionization potential due to the so-called "molecular field splitting."[59,60] For 2-tUra, the two S $2p_{3/2}$ levels are found at 168.01 and 168.13 eV and the S $2p_{1/2}$ level is found at 169.27 eV. In the case of 4-tUra, the values are 167.98 and 168.09 for S $2p_{3/2}$ and 169.24 eV for $2p_{1/2}$. The S $2p_{3/2}$ levels for 2,4-dtUra are found at 168.11 and 168.23 eV for the S_8 atom and 168.14 and 168.26 eV for the S_7 atom. The $2p_{1/2}$ levels are found at 169.37 and 169.40 eV for S_8 and S_7, respectively. Correlation satellites have not been included in the calculations. However, the offset of the measured maxima toward the main photoline falls in the range of valence excitations in these molecules[9] and shake-up satellites have also been observed in other sulfur containing molecules at this edge.[56,58]

A summary of the ionization energies of all edges for both experiment and calculations is given in Table I.

Near edge x-ray absorption fine structure

Oxygen 1s

The O 1s NEXAFS spectra of 2-tUra and 4-tUra are shown in Fig. 2. In both cases, a main resonant absorption is observed. For 2-tUra, this maximum is located at 531.3 eV, and for 4-tUra, it is located at 532.3 eV. The main feature is followed by a gradual increase of the signal. 4-tUra exhibits a shoulder-like feature at ~535.5 eV, and 2-tUra seems to show a more pronounced peak at similar energies. The theoretical calculations are in good agreement with the experiment after shifting them by 0.55 eV. The main absorption appears at 531.35 eV for 2-tUra and at 532.26 eV for 4-tUra. Additional resonances into Rydberg states are predicted at ~536 and 537.5 eV.

Considering the almost identical ionization energy for both molecules, the shift of the main excitation channel somewhat contrasts the valence spectra of these molecules where the first optical excitation in 4-tUra is redshifted to that of 2-tUra.[9] It appears that the lowest π^* orbital in 4-tUra shows no electron localization at the oxygen atom, which makes the transition dipole moment vanish. Hence, the electron is promoted into higher lying π^* orbitals. In contrast, the lowest π^* orbital in 2-tUra shows electron localization at the O atom and, thus, the resonant excitation can involve that orbital

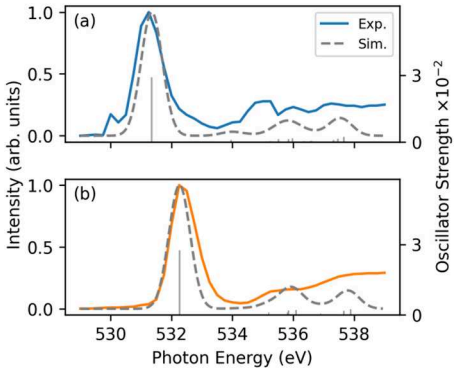

FIG. 2. Experimental (solid line) and theoretical (dashed line) NEXAFS spectra at the O 1s edge for (a) 2-tUra and (b) 4-tUra. The calculated core-to-valence transitions (sticks) have been broadened using a Gaussian line shape with $\sigma = 0.35$ eV in order to derive the theoretical spectrum (dashed line). The calculated spectra were shifted by 0.55 eV to match the main experimental absorption line. The values of the main transition are given in Tables II and IV.

leading to a lower excitation energy compared to its isomer. In the canonical nucleobases uracil and thymine, something similar can be observed.[61,62] There, the NEXAFS spectra at the O 1s edge show a strong double-peak pre-edge feature with a split of about 1 eV. Each of the peaks can be assigned to a transition from one of the O atoms to a π^* orbital with strong localization at the respective O atom.

Nitrogen 1s

Figure 3 shows the N 1s NEXAFS spectra of the three molecules. In the experiment, 2-tUra shows a first broad absorption at ~402 eV. This feature has a shoulder at about 401 eV, a peak at ~402 eV, and another peak at 403 eV. It is followed by a gradual increase in absorption with a shoulder at 404.5 eV and a peak at ~405.5 eV. 4-tUra shows a first resonance at 401 eV, followed by two more peaks at 403 and 405 eV. The first resonance for 2,4-dtUra is slightly shifted compared to that of 4-tUra and is located at ~401.5 eV. A second feature is observed at 403 eV and a broader band between 404 and 405.5 eV.

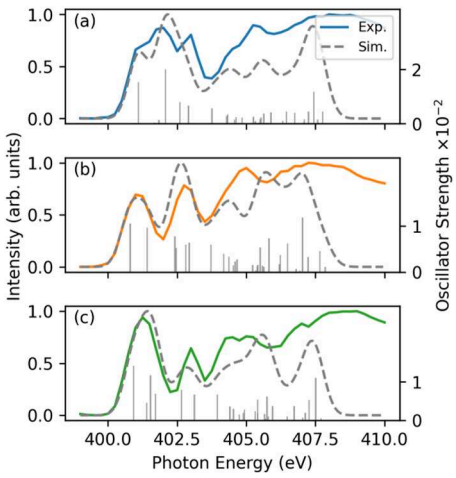

FIG. 3. Experimental (solid line) and theoretical (dashed line) NEXAFS spectra at N 1s edge for (a) 2-tUra, (b) 4-tUra, and (c) 2,4-dtUra. The calculated core-to-valence transitions (sticks) were broadened using a Gaussian line shape with $\sigma = 0.35$ eV in order to derive the theoretical spectrum (dashed line). The calculated spectra were shifted by −0.2 eV to match the first experimental absorption feature. The values for main transitions are given in Tables II, IV, and VI.

The ADC calculations again show similar features in the simulated spectrum. For 2-tUra, the first strong resonance is predicted to be at 401.1 eV and corresponds to a 1s $(N_3) \rightarrow \pi^*$ transition. This is followed by 1s $(N_1) \rightarrow \pi^*$ transition at 402.08 eV. At higher energies, the absorption bands are dominated by transitions into Rydberg states. The theoretical spectrum for 4-tUra shows two broad peaks at 401.2 and 402.5 eV, matching the experimental spectra. The first peak consists of two transitions from the 1s (N_1/N_3) to π^*/Rydberg-like states. Further resonance peaks occur at 404, 406, and 407 eV, which are described by transitions into Rydberg states. The spectrum for 2,4-dtUra shows a large absorption at 401.3 eV. This peak consists of different transitions from 1s (N_1/N_3) into the π^* orbital. Another resonance at 402.7 eV consists of transitions into σ^*/Rydberg-like states. At higher energies, the absorption is dominated by transitions into Rydberg states. In general, the NEXAFS spectra at the N 1s edge are fairly complex, including a large number of different transitions compared to the O 1s spectra, which showed a prominent pre-edge feature. The canonical nucleobases uracil and thymine also show a high density of transitions for the N 1s edge so that no pronounced pre-edge feature can be observed there either.[61,62]

Indeed, the agreement between the experimental and computed NEXAFS spectra worsens at photon energies higher than 406 eV. This is mainly due to the limited number of core-to-valence transitions explicitly accounted for in the ADC(2) calculations (including more states would make the computations unfeasible). Furthermore, at these energies, transitions to unbound electronic states (EXAFS), neglected by ADC(2), cannot be excluded.

Carbon 1s

The C 1s NEXAFS spectra are shown in Fig. 4. In contrast to the N 1s edge, the spectra show again well-defined pre-edge features. The first two absorption peaks observed are almost identical for all three molecules. They are located at ~284.8 and 286.2 eV. The third peak is located at ~287.7 eV for 2-tUra and 2,4-dtUra and at 288.8 eV for 4-tUra. However, the peak intensities vary. While the first peak is weakest in all three molecules, the highest peak for 2-tUra is the third one at 287.7 eV and, for 4-tUra, it is the second at 286.2 eV. In the case of 2,4-dtUra, the experiment does not show a significant difference between the second and third peaks.

The ADC calculations, again, resemble the experimental spectra very well after shifting the spectra by −0.4 eV. Three main absorptions are predicted for all three molecules. For 2-tUra, they are at 284.4, 286.1, and 288 eV, respectively. The first peak is a transition from the 1s orbital of C_5 to the π^* orbital, and the second is a transition from C_6 to the π^* orbital. The third peak combines transitions from C_4 and C_2 into π^*. For 4-tUra, the first peak is identical to 2-tUra. The second peak at 286.2 eV includes transitions from C_4, C_5, and C_6 to π^*. The last peak at 289.7 eV belongs to a transition from C_2 into π^*. For 2,4-dtUra, the first peak is also identical to that for 2-tUra. The second peak consists of different transitions from C_4, C_5, and C_6 into π^*. For the third peak, the main transition

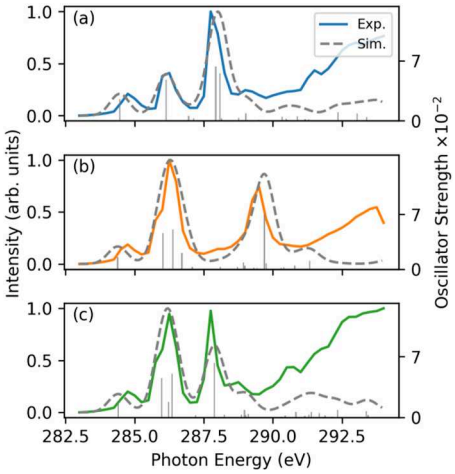

FIG. 4. Experimental (solid line) and theoretical (dashed line) NEXAFS spectra at C 1s edge for (a) 2-tUra, (b) 4-tUra, and (c) 2,4-dtUra. The calculated core-to-valence transitions (sticks) were broadened using a Gaussian line shape with $\sigma = 0.35$ eV in order to derive the theoretical spectrum (dashed line). The calculated spectra were shifted by −0.4 eV to match the second experimental absorption feature. The values for main transitions are given in Tables II, IV, and VI.

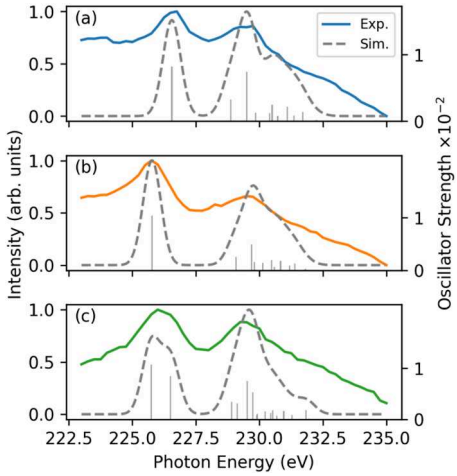

FIG. 5. Experimental (solid line) and theoretical (dashed line) NEXAFS spectra at S 2s edge for (a) 2-tUra, (b) 4-tUra, and (c) 2,4-dtUra. The calculated core-to-valence transitions (sticks) were broadened using a Gaussian line shape with $\sigma = 0.35$ eV in order to derive the theoretical spectrum (dashed line). The calculated spectra were shifted by 0.175 eV to match the first experimental absorption feature. The values for main transitions are shown in Tables II, IV, and VI.

originates from C_2 into π^*. For all three molecules, the order of the resonances follows the order of ionization energies for the individual carbon atoms.

Since only a limited number of core excited states are included in the ADC(2) calculations, the agreement between experimental and theoretical spectra worsens at photon energies higher than 291 eV, similarly to the case of the N 1s spectra.

In general, the spectra of the thionated uracils are very similar to the spectra of canonical pyrimidine-based nucleobases.[61,62] Both uracil and thymine also show very distinct absorption features at the C 1s that are attributed to excitations from one of the carbon atoms into the π^* orbital. The peaks of C_5 and C_6 are almost identical in position, which, however, might be expected as the oxygen substitution mostly affects C_2 and C_4.

Sulfur 2s

The sulfur 2s NEXAFS spectra are shown in Fig. 5. Above a stronger background, two main peaks are observable for all three molecules. The first peak is at 226.5 eV for 2-tUra, 225.7 eV for 4-tUra, and 226.1 eV for 2,4-dtUra. The second peak appears to be at almost the same position for all three molecules, i.e., 229 eV. The background may be due to a strong difference in signal between S 2s and S 2p features. The Coster–Kronig channels contributing to the enhancement of the electron yield signal overlap with the S 2p photoline and its satellites over the scanned energy range.

Two main absorption bands also appear in the ADC spectra. The first band is matched with experiment and, hence, located at 226.6 eV for 2-tUra, 225.8 eV for 4-tUra, and 225.8 eV for 2,4-dtUra with a shoulder at around 226.2 eV. The second band consists of multiple absorptions with a first peak at 229.5 eV. A shoulder occurs for all three molecules on the second band, which is located at around 231 eV for 2-tUra and 4-tUra and 231.5 eV for 2,4-dtUra.

The first observed peak at around 226.5 eV belongs to excitation(s) from the sulfur 2s orbital(s) to orbitals involving the lowest π^*-orbital. These usually exhibit significant electron density at the respective sulfur atoms. In the case of 2,4-dtUra, the first excitation, originating—with equal oscillator strength—from both sulfur atoms, is a combination of the two lowest π^* orbitals, which results in electron density at both sulfur atoms. The second observed peak

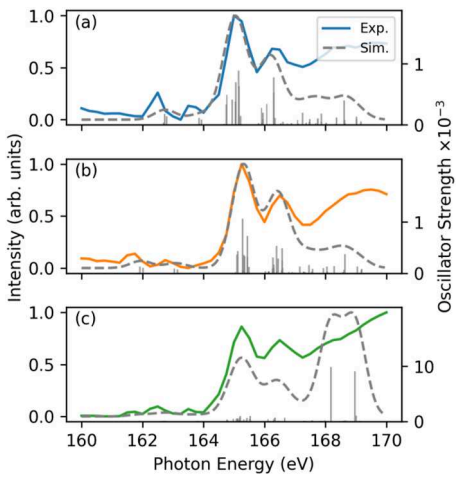

FIG. 6. Experimental (solid line) and theoretical (dashed line) NEXAFS spectra at the S 2p edge for (a) 2-tUra, (b) 4-tUra, and (c) 2,4-dtUra. The calculated core-to-valence transitions (sticks) were broadened using a Gaussian line shape with $\sigma = 0.35$ eV in order to derive the theoretical spectrum (dashed line). The calculated spectra were shifted by 0.125 eV to match the strongest experimental absorption feature. The values for main transitions are given in Tables III, V, and VII.

in the experimental spectrum at ~229 eV is dominated by transitions to σ*/Rydberg orbitals in all three molecules.

Similar observations of two pre-edge resonances have been made in the sulfur containing ring-molecules thiolane and thiophene as well.[63] Here, the maxima correspond to a mixture of π* and σ* excitation as well as to Rydberg states.

Sulfur 2p

In Fig. 6, the NEXAFS spectra of the S 2p edge are shown. Again, some similarities between the experimental spectra of the three thiouracils are observed. In particular, all show a double-peak structure around a photon energy of 166 eV. The peaks are located at 165.1 and 166.4 eV for 2-tUra, 165.3 and 166.5 eV for 4-tUra, and 165.2 and 166.5 eV for 2,4-dtUra. Interestingly, the splitting of the two peaks matches the SO-splitting observed in the photoelectron spectra. Two smaller peaks are also observed at lower photon energies. For 2-tUra, these are at 162.5 and 163.6 eV; for 4-tUra, at 161.6 and 162.7 eV; and for 2,4-dtUra, at 161.6 and 162.5 eV.

The CCSD calculations match the experimental data fairly well. The double peak structure at around 166 eV is reproduced for all

TABLE II. Calculated main transitions for 2-tUra NEXAFS spectra (C 1s, N 1s, O 1s, and S 2s). Shifts of 0.55, −0.2, −0.4, and 0.175 eV have been applied to the transitions at O 1s, N 1s, C 1s, and S 2s, respectively.

Energy (eV)	Oscillator strength	Main component	Exp. (eV)
226.56	0.008	2s (S_7) → π*	226.5
228.88	0.003	2s (S_7) → σ*/Ryd	229.0
229.51	0.007	2s (S_7) → σ*/Ryd	
284.46	0.025	1s (C_5) → π*	284.8
286.14	0.048	1s (C_6) → π*	286.2
287.93	0.063	1s (C_2) → π*	287.7
288.08	0.056	1s (C_4) → π*	
401.10	0.015	1s (N_3) → π*	401.2
402.08	0.020	1s (N_1) → π*	401.9
402.60	0.008	1s (N_1) → σ*/Ryd	402.9
407.44	0.012	1s (N_1) → Ryd	
531.35	0.029	1s (O_8) → π*	531.3

TABLE III. Calculated S 2p transitions for the 2-tUra NEXAFS spectrum shifted by 0.13. The transition energies account for spin–orbit coupling, and for each transition, the main components in the singlet and triplet manifolds are reported when their weight is larger than 0.1. The experimental peak maxima are also reported in the last column, in correspondence with the calculated transitions that most likely contribute to each peak.

Energy (eV)	Oscillator strength	Main singlet component (weight, transition)	Main triplet component (weight, transition, multiplicity)	Exp. (eV)
162.73	0.000 18	(0.56, $2p_x$ → π*)	(0.36, $2p_y$ → π*, M_S = 0)	162.5
162.80	0.000 14	(0.51, $2p_z$ → π*)	(0.48, $2p_x$ → π*, M_S = ±1)	
163.86	0.000 11	(0.41, $2p_x$ → π*)	(0.32, $2p_y$ → π*, M_S = 0)	163.6
163.94	0.000 09	(0.36, $2p_z$ → π*)		
164.75	0.000 34	(0.64, $2p_y$ → σ*)	(0.21, $2p_x$ → σ*, M_S = 0)	
164.77	0.000 49	(0.60, $2p_z$ → σ*)		
164.95	0.000 41	(0.48, $2p_x$ → σ*)		
165.05	0.000 38	(0.21, $2p_z$ → π*)	(0.70, $2p_y$ → Ryd, M_S = ±1)	
165.07	0.000 70	(0.29, $2p_z$ → π*)	(0.64, $2p_y$ → Ryd, M_S = ±1)	165.1
165.16	0.000 89	(0.33, $2p_z$ → π*)	(0.56, $2p_x$ → Ryd, M_S = 0)	
165.17	0.000 64	(0.41, $2p_y$ → π*)	(0.54, $2p_x$ → Ryd, M_S = ±1)	
165.22	0.000 15	(0.42, $2p_y$ → σ*)		
165.91	0.000 28	(0.19, $2p_z$ → σ*)		
166.08	0.000 35	(0.36, $2p_x$ → σ*)		
166.31	0.000 78	(0.30, $2p_z$ → π*)	(0.36, $2p_x$ → Ryd, M_S = 0)	
166.31	0.000 53	(0.33, $2p_z$ → π*)		166.4
166.35	0.000 11	(0.41, $2p_y$ → σ*)	(0.21, $2p_y$ → Ryd, M_S = 0)	
167.25	0.000 20	(0.43, $2p_x$ → Ryd)		
167.76	0.000 10	(0.27, $2p_y$ → σ*)		
167.87	0.000 18	(0.54, $2p_x$ → σ*)		
168.37	0.000 12	(0.29, $2p_x$ → σ*)	(0.27, $2p_y$ → Ryd, M_S = 0)	
168.62	0.000 40	(0.86, $2p_z$ → Ryd)		
169.02	0.000 14	(0.39, $2p_x$ → σ*)	(0.28, $2p_{yx}$ → Ryd, M_S = 0)	

TABLE IV. Calculated main transitions for 4-tUra NEXAFS spectra (C 1s, N 1s, O 1s, and S 2s). Shifts of 0.55, −0.2, −0.4, and 0.175 eV have been applied to the transitions at O 1s, N 1s, C 1s, and S 2s, respectively.

Energy (eV)	Oscillator strength	Main component	Exp. (eV)
225.78	0.010	2s (S_8) → π^*	225.7
229.08	0.003	2s (S_8) → σ^*/Ryd	229.0
229.70	0.005	2s (S_8) → σ^*/Ryd	
284.39	0.016	1s (C_5) → π^*	284.4
286.02	0.046	1s (C_6) → π^*	286.2
286.39	0.051	1s (C_4) → π^*	
286.71	0.021	1s (C_5) → π^*	288.8
289.69	0.070	1s (C_2) → π^*	
400.80	0.011	1s (N_3) → π^*/Ryd	401.1
401.42	0.010	1s (N_1) → π^*/Ryd	
402.42	0.008	1s (N_1) → σ^*/Ryd	402.8
402.46	0.005	1s (N_3) → π^*/Ryd	
402.81	0.006	1s (N_1) → π^*/Ryd	
402.93	0.006	1s (N_3) → σ^*/Ryd	
403.72	0.006	1s (N_3) → σ^*/Ryd	
405.50	0.005	1s (N_3) → π^*	405.0
405.82	0.007	1s (N_1) → π^*	
406.49	0.006	1s (N_1) → σ^*/Ryd	
407.03	0.012	1s (N_1) → σ^*/Ryd	
532.26	0.028	1s (O_7) → π^*	532.3

TABLE VI. Calculated main transitions for 2,4-dtUra NEXAFS spectra (C 1s, N 1s, and S 2s). Shifts of −0.2, −0.4, and 0.175 eV have been applied to the transitions at N 1s, C 1s, and S 2s, respectively.

Energy (eV)	Oscillator strength	Main component	Exp. (eV)
225.75	0.011	2s (S_8) → π^*	226.1
226.51	0.008	2s (S_7) → π^*	
228.91	0.003	2s (S_7) → σ^*/Ryd	229.0
229.13	0.003	2s (S_8) → σ^*/Ryd	
229.53	0.008	2s (S_7) → σ^*/Ryd	
229.75	0.005	2s (S_8) → σ^*/Ryd	
284.40	0.018	1s (C_5) → π^*	284.8
285.98	0.045	1s (C_6) → π^*	286.2
286.22	0.018	1s (C_5) → π^*	
286.35	0.050	1s (C_4) → π^*	
287.88	0.063	1s (C_2) → π^*	287.7
400.93	0.014	1s (N_3) → π^*	401.2
401.54	0.012	1s (N_1) → π^*	
401.71	0.007	1s (N_1) → π^*	
402.65	0.008	1s (N_1) → σ^*/Ryd	403.0
403.13	0.007	1s (N_3) → σ^*/Ryd	
403.96	0.007	1s (N_3) → σ^*/Ryd	404.8
405.41	0.005	1s (N_3) → π^*/Ryd	
405.75	0.006	1s (N_1) → π^*/Ryd	
407.27	0.005	1s (N_1) → σ^*/Ryd	
407.51	0.011	1s (N_1) → σ^*/Ryd	

TABLE V. Calculated S 2p transitions for the 4-tUra NEXAFS spectrum shifted by 0.13 eV. The transition energies account for spin–orbit coupling, and for each transition, the main components in the singlet and triplet manifolds are reported when their weight is larger than 0.1. The experimental peak maxima are also reported in the last column, in correspondence with the calculated transitions that most likely contribute to each peak.

Energy (eV)	Oscillator strength	Main singlet component (weight, transition)	Main triplet component (weight, transition, multiplicity)	Exp. (eV)
161.92	0.000 13	(0.55, $2p_x \rightarrow \pi^*$)	(0.37, $2p_y \rightarrow \pi^*$, $M_S = 0$)	161.6
162.02	0.000 11	(0.54, $2p_z \rightarrow \pi^*$)	(0.44, $2p_x \rightarrow \pi^*$, $M_S = \pm 1$)	
163.05	0.000 10	(0.43, $2p_x \rightarrow \pi^*$)	(0.31, $2p_y \rightarrow \pi^*$, $M_S = 0$)	162.7
163.15	0.000 08	(0.39, $2p_z \rightarrow \pi^*$)		
165.10	0.000 37	(0.65, $2p_y \rightarrow \sigma^*$)		
165.13	0.000 44	(0.59, $2p_z \rightarrow \sigma^*$)		
165.29	0.001 06	(0.48, $2p_y \rightarrow$ Ryd)		
165.33	0.000 35		(0.70, $2p_y \rightarrow$ Ryd, $M_S = \pm 1$)	165.3
165.35	0.000 33		(0.62, $2p_z \rightarrow$ Ryd, $M_S = \pm 1$)	
165.44	0.000 31		(0.58, $2p_x \rightarrow \sigma^*$, $M_S = 0$)	
165.45	0.000 73	(0.44, $2p_z \rightarrow \sigma^*$)	(0.52, $2p_x \rightarrow$ Ryd, $M_S = \pm 1$)	
166.28	0.000 31	(0.21, $2p_z \rightarrow \sigma^*$)		
166.40	0.000 53	(0.38, $2p_x \rightarrow$ Ryd)	(0.12, $2p_y \rightarrow \sigma^*$, $M_S = 0$)	
166.45	0.000 29	(0.36, $2p_x \rightarrow$ Ryd)		166.5
166.59	0.000 26		(0.30, $2p_y \rightarrow \pi^*$, $M_S = 0$)	
166.59	0.000 53	(0.29, $2p_z \rightarrow \sigma^*$)		
168.64	0.000 37	(0.96, $2p_z \rightarrow \sigma^*$/Ryd)		

TABLE VII. Calculated S 2p transitions for the 2,4-dtUra NEXAFS spectrum shifted by 0.13 eV. The transition energies account for spin–orbit coupling, and for each transition, the main components in the singlet and triplet manifolds are reported when their weight is larger than 0.1. The experimental peak maxima are also reported in the last column, in correspondence with the calculated transitions that most likely contribute to each peak.

Energy (eV)	Oscillator strength	Main singlet component (weight, transition)	Main triplet component (weight, transition, multiplicity)	Exp. (eV)
161.89	0.000 13	[0.55, $2p_x$ (S_8) → π*]	[0.37, $2p_y$ (S_8) → π*, M_S = 0]	161.6
162.00	0.000 10	[0.54, $2p_z$ (S_8) → π*]	[0.44, $2p_x$ (S_8) → π*, M_S = ±1]	
162.68	0.000 17	[0.56, $2p_x$ (S_7) → π*]	[0.37, $2p_y$ (S_7) → π*, M_S = 0]	
162.75	0.000 13	[0.52, $2p_z$ (S_7) → π*]	[0.48, $2p_x$ (S_7) → π*, M_S = ±1]	162.4
163.02	0.000 10	[0.43, $2p_x$ (S_8) → π*]	[0.31, $2p_y$ (S_8) → π*, M_S = 0]	
163.13	0.000 08	[0.40, $2p_z$ (S_8) → π*]		
163.81	0.000 12	[0.41, $2p_x$ (S_7) → π*]	[0.32, $2p_y$ (S_7) → π*, M_S = 0]	163.5
163.89	0.000 10	[0.37, $2p_z$ (S_7) → π*]		
164.77	0.000 40	[0.64, $2p_y$ (S_7) → σ*]		
164.98	0.000 49	[0.46, $2p_x$ (S_7) → σ*]		
165.09	0.000 49	[0.22, $2p_z$ (S_7) → σ*]	[0.70, $2p_y$ (S_7) → Ryd, M_S = ±1]	
165.11	0.000 61	[0.30, $2p_y$ (S_7) → Ryd]	[0.64, $2p_z$ (S_7) → Ryd, M_S = ±1]	
165.13	0.000 62	[0.65, $2p_y$ (S_8) → σ*]		165.2
165.20	0.000 75	[0.32, $2p_y$ (S_7) → Ryd]	[0.56, $2p_x$ (S_7) → Ryd, M_S = 0]	
165.21	0.000 99	[0.40, $2p_z$ (S_7) → σ*/Ryd]	[0.54, $2p_x$ (S_7) → Ryd, M_S = ±1]	
165.43	0.000 66	[0.32, $2p_y$ (S_8) → Ryd]	[0.60, $2p_z$ (S_8) → Ryd, M_S = ±1]	
165.54	0.001 02	[0.43, $2p_z$ (S_8) → σ*/Ryd]	[0.54, $2p_x$ (S_8) → Ryd, M_S = ±1]	
166.12	0.000 47	[0.34, $2p_x$ (S_7) → σ*]		
166.31	0.000 47	[0.28, $2p_y$ (S_8) → σ*]	[0.26, $2p_x$ (S_8) → σ*, M_S = 0]	
166.35	0.000 64	(0.30, $2p_y$ (S_7) → Ryd)	[0.36, $2p_x$ (S_7) → Ryd, M_S = 0]	166.5
166.35	0.000 76	[0.33, $2p_z$ (S_7) → σ*/Ryd]		
166.67	0.000 54	[0.27, $2p_y$ (S_8) → Ryd]	[0.35, $2p_x$ (S_8) → Ryd, M_S = 0]	
166.67	0.000 77	[0.33, $2p_z$ (S_8) → σ*/Ryd]		
168.18	0.009 85	[0.49, $2p_y$ (S_7) → σ*/Ryd]	[0.25, $2p_z$ (S_7) → σ*/Ryd, M_S = 0]	
168.97	0.009 11	[0.45, $2p_y$ (S_7) → σ*/Ryd]	[0.42, $2p_z$ (S_7) → σ*/Ryd, M_S = ±1]	
169.01	0.001 13	[0.26, $2p_z$ (S_7) → Ryd]	[0.34, $2p_x$ (S_7) → Ryd, M_S = ±1]	

TABLE VIII. Monochromator and hemisphere parameters for the XPS measurements.

			Monochromator		Hemispherical analyzer			
	Edge	E_{phot} (eV)	Slit size (μm)	Resolution (meV)	E_{pass} (ev)	Slit	Resolution (meV)	Total res. (meV)
2-tUra	S 2p	250	50	57	50	500	62.5	84.6
	S 2s	330	100	172	100	500	236	212.6
	C 1s	382	100	212	20	500	25	213.5
	N 1s	495	100	306	50	500	62.5	312.3
	O 1s	628	100	435	100	500	236	494.9
4-tUra	S 2p	250	100	110	50	500	62.5	126.5
	S 2s	330	100	172	100	500	125	21.6
	C 1s	382	50	110	50	500	62.5	126.5
	N 1s	495	50	158	100	500	125	201.5
	O 1s	628	100	435	50	500	62.5	439.5
2,4-dtUra	S 2p	250	50	57	50	500	62.5	84.6
	S 2s	330	50	110	100	500	125	166.5
	C 1s	382	20	53	50	500	62.5	81.9
	N 1s	495	100	306	200	500	250	395.1

TABLE IX. Monochromator parameters for the NEXAFS measurements.

	Edge	Slit size (μm)	Resolution (meV)
2-tUra	S 2p	200	120
	S 2s	250	248
	C 1s	175	250
	N 1s	100	225
	O 1s	75	256
4-tUra	S 2p	220	125
	S 2s	250	248
	C 1s	200	268
	N 1s	100	230
	O 1s	75	256
2,4-dtUra	S 2p	100	70
	S 2s	250	250
	C 1s	200	266
	N 1s	100	233

three molecules and is found to be due to the 1/2–3/2 spin–orbit splitting (it is absent in non-relativistic calculations). The transitions contributing to the intensity in this energy range involve virtual σ^* orbitals mainly localized on the C=S bonds, diffuse Rydberg orbitals (only for 4-tUra and 2,4-dtUra), and a π^* orbital localized on the C=C bond (only for 2-tUra and 4-tUra). The small peaks between 162 and 164 eV are reproduced as well and can be attributed to transitions into π^* orbitals with a large lobe on the C=S bonds. For 2,4-dtUra, the calculations give two very strong lines around the ionization edge, which do not occur in the other two molecules, and are due to transitions to diffuse Rydberg orbitals.

Similarly to other edges, the density of states increases considerably for photon energies higher than 167 eV. Therefore, the calculated spectra, which include only a limited number of transitions, fail in reproducing the full intensity observed experimentally. Notably, the calculation for 2,4-dtUra predict two strong transitions at around 169 eV, which involve a virtual Rydberg orbital and the 2p electrons near the S7 atom, and are not visible in the experiment. This discrepancy is possibly due to a shorter lifetime of these states (expected by the high density of states) that leads to broader bands or due to an overestimation of the intensity by the EOM-CCSD calculations.

Other sulfur containing ring-like molecules, such as thiophene, also show distinct pre-edge features in the NEXAFS spectrum that are dominated by the spin–orbit split character of the S 2p orbitals.[63,64] Similar to thiouracils, the main features are also described by a mixture of transitions into σ^*, π^*, and diffuse Rydberg orbitals.[64] Interestingly, the weaker features dominated by π^* transitions have not been observed in these studies.

CONCLUSION

We reported the x-ray photoelectron and NEXAFS spectra of 2-thiouracil, 4-thiouracil, and 2,4-dithiouracil in the gas phase. While core-level electron spectra and some absorption spectra of 2-thiouracil have been reported previously,[27,28,32,33] to the best of our knowledge, no spectra of the other two thiouracils have been reported before. Hence, this study provides the first overview of the ground-state core-level spectroscopy of these molecules. Furthermore, it may serve as a prerequisite for more advanced, time-resolved x-ray studies to investigate the photodynamics of thiobases.

Coupled-cluster and ADC(2) calculations were performed to identify the excitation channels. The calculated spectra, in good agreement with experimental data, extend the literature dataset of theoretical core level spectra computed via coupled-cluster or ADC(2), confirm the validity of these methods for medium-sized molecules, and provide benchmark results to validate computationally cheaper approaches (e.g., linear response or transition potential density functional theory) applicable to larger molecular systems.

ACKNOWLEDGMENTS

The spectra were recorded at the PLEIADES beamline at the synchrotron SOLEIL, France, under proposal Grant Nos. 20200549 and 20211636. We acknowledge SOLEIL for provision of synchrotron radiation facilities, and we would like to thank E. Robert and C. Nicolas for their technical assistance during the beamtime at PLEIADES. We thank Volkswagen foundation for funding via a Lichtenberg Professorship. We thank BMBF for funding via Verbundforschungsprojekt Grant No. 05K19IP1. We acknowledge DFG funding via Grant Nos. GU 1478/1-1 (M. G.) and SA 547/17-1 (P. S.) via the common Project No. 445713302.

AUTHOR DECLARATIONS

Conflict of Interest

The authors have no conflicts to disclose.

Author Contributions

Dennis Mayer: Data curation (equal); Formal analysis (equal); Investigation (equal); Validation (equal); Visualization (equal); Writing – original draft (equal); Writing – review & editing (equal). **Max Handrich**: Data curation (equal); Formal analysis (equal); Investigation (equal); Methodology (equal); Software (equal); Visualization (equal); Writing – review & editing (equal). **David Picconi**: Data curation (equal); Formal analysis (equal); Investigation (equal); Methodology (equal); Software (equal); Visualization (equal); Writing – original draft (equal); Writing – review & editing (equal). **Fabiano Lever**: Data curation (equal); Formal analysis (equal); Investigation (equal); Methodology (equal); Software (equal); Visualization (equal); Writing – original draft (equal); Writing – review & editing (equal). **Lisa Mehner**: Investigation (equal); Writing – review & editing (equal). **Marta L. Murillo-Sanchez**: Investigation (equal); Writing – review & editing (equal). **Constantin Walz**: Investigation (equal); Writing – review & editing (equal). **Evgenii Titov**: Formal analysis (equal); Investigation (equal); Methodology (equal); Supervision (equal); Writing – review & editing (equal). **John Bozek**: Formal analysis (equal); Investigation (equal); Methodology (equal); Resources (equal); Supervision (equal); Writing – review & editing (equal). **Peter Saalfrank**: Formal analysis (equal); Funding acquisition (equal);

Investigation (equal); Project administration (equal); Resources (equal); Supervision (equal); Writing – review & editing (equal). **Markus Gühr**: Conceptualization (equal); Formal analysis (equal); Funding acquisition (equal); Investigation (equal); Project administration (equal); Supervision (equal); Writing – review & editing (equal).

DATA AVAILABILITY

The data that support the findings of this study are available from the corresponding author upon reasonable request.

APPENDIX: ASSIGNMENTS OF NEXAFS TRANSITIONS

Here, we report the assignment of the most intense NEXAFS transitions, together with the experimental energies of the peak maxima. For the transitions at the highest photon energies, clear experimental peaks cannot be neatly discerned, due to the high density of states.

For ADC(2) calculations (C 1s, N 1s, O 1s, and S 2s edges), the assignment is based on the largest coefficient in the ADC(2) wave function for the (singlet) core-excited states, with respect to the basis of canonical Hartree–Fock orbitals, as usual.

At the S 2p edge, the core-excited states have a mixed singlet-triplet character; therefore, the assignment follows a different procedure. First, for each state, the dominant singlet and triplet transitions are identified, with the latter included only when its weight is higher than 0.1. Then, for each spin-pure transition, the dominant pair of natural transition orbitals[65] is used for the assignment. The weights reported in Tables S2, S4, and S6 indicate the degree of singlet–triplet mixing.

REFERENCES

[1] T. Carell, C. Brandmayr, A. Hienzsch, M. Müller, D. Pearson, V. Reiter, I. Thoma, P. Thumbs, and M. Wagner, "Structure and function of noncanonical nucleobases," Angew. Chem., Int. Ed. **51**(29), 7110–7131 (2012).

[2] S. Arslancan, L. Martínez-Fernández, and I. Corral, "Photophysics and photochemistry of canonical nucleobases' thioanalogs: From quantum mechanical studies to time resolved experiments," Molecules **22**(6), 998 (2017).

[3] B. Ashwood, M. Pollum, and C. E. Crespo-Hernández, "Photochemical and photodynamical properties of sulfur-substituted nucleic acid bases," Photochem. Photobiol. **95**(1), 33–58 (2019).

[4] W. J. Schreier, T. E. Schrader, F. O. Koller, P. Gilch, C. E. Crespo-Hernández, V. N. Swaminathan, T. Carell, W. Zinth, and B. Kohler, "Thymine dimerization in DNA is an ultrafast photoreaction," Science **315**(5812), 625–629 (2007).

[5] G. B. Elion, W. S. Ide, and G. H. Hitchings, "The ultraviolet absorption spectra of thiouracils[1]," J. Am. Chem. Soc. **68**(11), 2137–2140 (1946).

[6] N. Igarashi-Yamamoto, A. Tajiri, M. Hatano, S. Shibuya, and T. Ueda, "Ultraviolet absorption, circular dichroism and magnetic circular dichroism studies of sulfur-containing nucleic acid bases and their nucleosides," Biochim. Biophys. Acta, Nucleic Acids Protein Synth. **656**(1), 1–15 (1981).

[7] H. Rostkowska, A. Barski, K. Szczepaniak, M. Szczesniak, and W. B. Person, "The tautomeric equilibria of thioanalogues of nucleic acids: Spectroscopic studies of 2-thiouracils in the vapour phase and in low temperature matrices," J. Mol. Struct. **176**, 137–147 (1988).

[8] A. Khvorostov, L. Lapinski, H. Rostkowska, and M. J. Nowak, "UV-Induced generation of rare tautomers of 2-thiouracils: A matrix isolation study," J. Phys. Chem. A **109**(34), 7700–7707 (2005).

[9] D. Mayer, D. Picconi, M. S. Robinson, and M. Gühr, "Experimental and theoretical gas-phase absorption spectra of thionated uracils," Chem. Phys. **558**, 111500 (2022).

[10] O. Ghafur, S. W. Crane, M. Ryszka, J. Bockova, A. Rebelo, L. Saalbach, S. De Camillis, J. B. Greenwood, S. Eden, and D. Townsend, "Ultraviolet relaxation dynamics in uracil: Time-resolved photoion yield studies using a laser-based thermal desorption source," J. Chem. Phys. **149**(3), 034301 (2018).

[11] J. A. Sánchez-Rodríguez, A. Mohamadzade, S. Mai, B. Ashwood, M. Pollum, P. Marquetand, L. González, C. E. Crespo-Hernández, and S. Ullrich, "2-Thiouracil intersystem crossing photodynamics studied by wavelength-dependent photoelectron and transient absorption spectroscopies," Phys. Chem. Chem. Phys. **19**(30), 19756–19766 (2017).

[12] H. Yu, J. A. Sanchez-Rodriguez, M. Pollum, C. E. Crespo-Hernández, S. Mai, P. Marquetand, L. González, and S. Ullrich, "Internal conversion and intersystem crossing pathways in UV excited, isolated uracils and their implications in prebiotic chemistry," Phys. Chem. Chem. Phys. **18**(30), 20168–20176 (2016).

[13] R. Borrego-Varillas, D. C. Teles-Ferreira, A. Nenov, I. Conti, L. Ganzer, C. Manzoni, M. Garavelli, A. Maria de Paula, and G. Cerullo, "Observation of the sub-100 femtosecond population of a dark state in a thiobase mediating intersystem crossing," J. Am. Chem. Soc. **140**(47), 16087–16093 (2018).

[14] X. Zou, X. Dai, K. Liu, H. Zhao, D. Song, and H. Su, "Photophysical and photochemical properties of 4-thiouracil: Time-resolved IR spectroscopy and DFT studies," J. Phys. Chem. B **118**(22), 5864–5872 (2014).

[15] D. Koyama, M. J. Milner, and A. J. Orr-Ewing, "Evidence for a double well in the first triplet excited state of 2-thiouracil," J. Phys. Chem. B **121**(39), 9274–9280 (2017).

[16] D. C. Teles-Ferreira, I. Conti, R. Borrego-Varillas, A. Nenov, I. H. M. M. Van Stokkum, L. Ganzer, C. Manzoni, A. M. de Paula, G. Cerullo, M. Garavelli, D. C. Teles-Ferreira, I. Conti, R. Borrego-Varillas, A. Nenov, I. H. M. M. Van Stokkum, L. Ganzer, C. Manzoni, A. M. de Paula, G. Cerullo, and M. Garavelli, "A unified experimental/theoretical description of the ultrafast photophysics of single and double thionated uracils," Chem.-Eur. J. **26**(1), 336–343 (2020).

[17] D. C. Teles-Ferreira, I. H. M. van Stokkum, I. Conti, L. Ganzer, C. Manzoni, M. Garavelli, G. Cerullo, A. Nenov, R. Borrego Varillas, and A. M. de Paula, "Coherent vibrational modes promote the ultrafast internal conversion and intersystem crossing in thiobases," Phys. Chem. Chem. Phys. **24**, 21750 (2022).

[18] A. Mohamadzade, S. Bai, M. Barbatti, and S. Ullrich, "Intersystem crossing dynamics in singly substituted thiouracil studied by time-resolved photoelectron spectroscopy: Micro-environmental effects due to sulfur position," Chem. Phys. **515**, 572–579 (2018).

[19] A. Mohamadzade and S. Ullrich, "Internal conversion and intersystem crossing dynamics of uracil upon double thionation: A time-resolved photoelectron spectroscopy study in the gas phase," Phys. Chem. Chem. Phys. **22**(27), 15608–15615 (2020).

[20] A. Mohamadzade, A. Nenov, M. Garavelli, I. Conti, and S. Ullrich, "Double thionated pyrimidine nucleobases: Molecular tools with tunable photoproperties," J. Am. Chem. Soc. **145**(22), 11945–11958 (2023).

[21] M. S. Robinson, M. Niebuhr, and M. Gühr, "Ultrafast photo-ion probing of the relaxation dynamics in 2-thiouracil," Molecules **28**(5), 2354 (2023).

[22] M. Ruckenbauer, S. Mai, P. Marquetand, and L. González, "Photoelectron spectra of 2-thiouracil, 4-thiouracil, and 2,4-dithiouracil," J. Chem. Phys. **144**(7), 074303 (2016).

[23] S. Mai, P. Marquetand, and L. González, "A static picture of the relaxation and intersystem crossing mechanisms of photoexcited 2-thiouracil," J. Phys. Chem. A **119**(36), 9524–9533 (2015).

[24] M. K. Shukla and J. Leszczynski, "Multiconfigurational self-consistent field study of the excited state properties of 4-thiouracil in the gas phase," J. Phys. Chem. A **108**(35), 7241–7246 (2004).

[25] M. K. Shukla and J. Leszczynski, "Electronic transitions of thiouracils in the gas phase and in solutions: Time-dependent density functional theory (TD-DFT) study," J. Phys. Chem. A **108**(46), 10367–10375 (2004).

[26] J. P. Gobbo and A. C. Borin, "2-Thiouracil deactivation pathways and triplet states population," Comput. Theor. Chem. **1040–1041**, 195–201 (2014).

[27] D. Mayer, F. Lever, D. Picconi, J. Metje, S. Alisauskas, F. Calegari, S. Düsterer, C. Ehlert, R. Feifel, M. Niebuhr, B. Manschwetus, M. Kuhlmann, T. Mazza, M. S. Robinson, R. J. Squibb, A. Trabattoni, M. Wallner, P. Saalfrank, T. J. A. Wolf,

and M. Gühr, "Following excited-state chemical shifts in molecular ultrafast x-ray photoelectron spectroscopy," Nat. Commun. **13**(1), 198 (2022).
[28]F. Lever, D. Mayer, D. Picconi, J. Metje, S. Alisauskas, F. Calegari, S. Düsterer, C. Ehlert, R. Feifel, M. Niebuhr, B. Manschwetus, M. Kuhlmann, T. Mazza, M. S. Robinson, R. J. Squibb, A. Trabattoni, M. Wallner, P. Saalfrank, T. J. A. Wolf, and M. Gühr, "Ultrafast dynamics of 2-thiouracil investigated by time-resolved Auger spectroscopy," J. Phys. B: At., Mol. Opt. Phys. **54**(1), 014002 (2020).
[29]B. K. McFarland, J. P. Farrell, S. Miyabe, F. Tarantelli, A. Aguilar, N. Berrah, C. Bostedt, J. D. Bozek, P. H. Bucksbaum, J. C. Castagna, R. N. Coffee, J. P. Cryan, L. Fang, R. Feifel, K. J. Gaffney, J. M. Glownia, T. J. Martinez, M. Mucke, B. Murphy, A. Natan, T. Osipov, V. S. Petrović, S. Schorb, T. Schultz, L. S. Spector, M. Swiggers, I. Tenney, S. Wang, J. L. White, W. White, and M. Gühr, "Ultrafast X-ray Auger probing of photoexcited molecular dynamics," Nat. Commun. **5**(1), 4235–4237 (2014).
[30]T. J. A. A. Wolf, R. H. Myhre, J. P. Cryan, S. Coriani, R. J. Squibb, A. Battistoni, N. Berrah, C. Bostedt, P. Bucksbaum, G. Coslovich, R. Feifel, K. J. Gaffney, J. Grilj, T. J. Martinez, S. Miyabe, S. P. Moeller, M. Mucke, A. Natan, R. Obaid, T. Osipov, O. Plekan, S. Wang, H. Koch, and M. Gühr, "Probing ultrafast $\pi\pi^*/n\pi^*$ internal conversion in organic chromophores via K-edge resonant absorption," Nat. Commun. **8**(1), 29 (2017).
[31]D. Mayer, F. Lever, and M. Gühr, "Time-resolved x-ray spectroscopy of nucleobases and their thionated analogs," Photochem. Photobiol. **100**(2), 275–290 (2024).
[32]B. M. Giuliano, V. Feyer, K. C. Prince, M. Coreno, L. Evangelisti, S. Melandri, and W. Caminati, "Tautomerism in 4-hydroxypyrimidine, S-methyl-2-thiouracil, and 2-thiouracil," J. Phys. Chem. A **114**(48), 12725–12730 (2010).
[33]F. Lever, D. Mayer, J. Metje, S. Alisauskas, F. Calegari, S. Düsterer, R. Feifel, M. Niebuhr, B. Manschwetus, M. Kuhlmann, T. Mazza, M. S. Robinson, R. J. Squibb, A. Trabattoni, M. Wallner, T. J. A. Wolf, and M. Gühr, "Core-level spectroscopy of 2-thiouracil at the sulfur L_1- and $L_{2,3}$-edges utilizing a SASE free-electron laser," Molecules **26**(21), 6469 (2021).
[34]D. Mayer, F. Lever, and M. Gühr, "Data analysis procedures for time-resolved x-ray photoelectron spectroscopy at a SASE free-electron-laser," J. Phys. B: At., Mol. Opt. Phys. **55**(5), 054002 (2022).
[35]Y. Nam, F. Montorsi, D. Keefer, S. M. Cavaletto, J. Y. Lee, A. Nenov, M. Garavelli, and S. Mukamel, "Time-resolved optical pump-resonant X-ray probe spectroscopy of 4-thiouracil: A simulation study," J. Chem. Theory Comput. **18**, 3075 (2022).
[36]See https://www.synchrotron-soleil.fr/en/beamlines/pleiades for a description of the PLEIADES beamline at SOLEIL.
[37]M. A. V. Ribeiro da Silva, L. M. P. F. Amaral, and P. Szterner, "Experimental study on the thermochemistry of 2-thiouracil, 5-methyl-2-thiouracil and 6-methyl-2-thiouracil," J. Chem. Thermodyn. **57**, 380–386 (2013).
[38]T. Clark, J. Chandrasekhar, G. W. Spitznagel, and P. V. R. Schleyer, "Efficient diffuse function-augmented basis sets for anion calculations. III. The 3-21+G basis set for first-row elements, Li–F," J. Comput. Chem. **4**(3), 294–301 (1983).
[39]G. W. Spitznagel, T. Clark, P. von Ragué Schleyer, and W. J. Hehre, "An evaluation of the performance of diffuse function-augmented basis sets for second row elements, Na–Cl," J. Comput. Chem. **8**(8), 1109–1116 (1987).
[40]Y. Shao, Z. Gan, E. Epifanovsky, A. T. B. Gilbert, M. Wormit, J. Kussmann, A. W. Lange, A. Behn, J. Deng, X. Feng, D. Ghosh, M. Goldey, P. R. Horn, L. D. Jacobson, I. Kaliman, R. Z. Khaliullin, T. Kuś, A. Landau, J. Liu, E. I. Proynov, Y. M. Rhee, R. M. Richard, M. A. Rohrdanz, R. P. Steele, E. J. Sundstrom, H. L. Woodcock, P. M. Zimmerman, D. Zuev, B. Albrecht, E. Alguire, B. Austin, G. J. O. Beran, Y. A. Bernard, E. Berquist, K. Brandhorst, K. B. Bravaya, S. T. Brown, D. Casanova, C.-M. Chang, Y. Chen, S. H. Chien, K. D. Closser, D. L. Crittenden, M. Diedenhofen, R. A. DiStasio, H. Do, A. D. Dutoi, R. G. Edgar, S. Fatehi, L. Fusti-Molnar, A. Ghysels, A. Golubeva-Zadorozhnaya, J. Gomes, M. W. D. Hanson-Heine, P. H. P. Harbach, A. W. Hauser, E. G. Hohenstein, Z. C. Holden, T.-C. Jagau, H. Ji, B. Kaduk, K. Khistyaev, J. Kim, J. Kim, R. A. King, P. Klunzinger, D. Kosenkov, T. Kowalczyk, C. M. Krauter, K. U. Lao, A. D. Laurent, K. V. Lawler, S. V. Levchenko, C. Y. Lin, F. Liu, E. Livshits, R. C. Lochan, A. Luenser, P. Manohar, S. F. Manzer, S.-P. Mao, N. Mardirossian, A. V. Marenich, S. A. Maurer, N. J. Mayhall, E. Neuscamman, C. M. Oana, R. Olivares-Amaya, D. P. O'Neill, J. A. Parkhill, T. M. Perrine, R. Peverati, A. Prociuk, D. R. Rehn, E. Rosta, N. J. Russ, S. M. Sharada, S. Sharma, D. W. Small, A. Sodt, T. Stein, D. Stück, Y.-C. Su, A. J. W. Thom, T. Tsuchimochi, V. Vanovschi, L. Vogt, O. Vydrov, T. Wang, M. A. Watson, J. Wenzel, A. White, C. F. Williams, J. Yang, S. Yeganeh, S. R. Yost, Z.-Q. You, I. Y. Zhang, X. Zhang, Y. Zhao, B. R. Brooks, G. K. L. Chan, D. M. Chipman, C. J. Cramer, W. A. Goddard, M. S. Gordon, W. J. Hehre, A. Klamt, H. F. Schaefer, M. W. Schmidt, C. D. Sherrill, D. G. Truhlar, A. Warshel, X. Xu, A. Aspuru-Guzik, R. Baer, A. T. Bell, N. A. Besley, J.-D. Chai, A. Dreuw, B. D. Dunietz, T. R. Furlani, S. R. Gwaltney, C.-P. Hsu, Y. Jung, J. Kong, D. S. Lambrecht, W. Liang, C. Ochsenfeld, V. A. Rassolov, L. V. Slipchenko, J. E. Subotnik, T. Van Voorhis, J. M. Herbert, A. I. Krylov, P. M. W. Gill, and M. Head-Gordon, "Advances in molecular quantum chemistry contained in the Q-Chem 4 program package," Mol. Phys. **113**(2), 184–215 (2015).
[41]M. L. Vidal, X. Feng, E. Epifanovsky, A. I. Krylov, and S. Coriani, "New and efficient equation-of-motion coupled-cluster framework for core-excited and core-ionized states," J. Chem. Theory Comput. **15**(5), 3117–3133 (2019).
[42]M. L. Vidal, P. Pokhilko, A. I. Krylov, and S. Coriani, "Equation-of-motion coupled-cluster theory to model L-edge X-ray absorption and photoelectron spectra," J. Phys. Chem. Lett. **11**(19), 8314–8321 (2020).
[43]P. Pokhilko, E. Epifanovsky, and A. I. Krylov, "General framework for calculating spin–orbit couplings using spinless one-particle density matrices: Theory and application to the equation-of-motion coupled-cluster wave functions," J. Chem. Phys. **151**(3), 034106 (2019).
[44]E. Epifanovsky, A. T. B. Gilbert, X. Feng, J. Lee, Y. Mao, N. Mardirossian, P. Pokhilko, A. F. White, M. P. Coons, A. L. Dempwolff, Z. Gan, D. Hait, P. R. Horn, L. D. Jacobson, I. Kaliman, J. Kussmann, A. W. Lange, K. U. Lao, D. S. Levine, J. Liu, S. C. McKenzie, A. F. Morrison, K. D. Nanda, F. Plasser, D. R. Rehn, M. L. Vidal, Z.-Q. You, Y. Zhu, B. Alam, B. J. Albrecht, A. Aldossary, E. Alguire, J. H. Andersen, V. Athavale, D. Barton, K. Begam, A. Behn, N. Bellonzi, Y. A. Bernard, E. J. Berquist, H. G. A. Burton, A. Carreras, K. Carter-Fenk, R. Chakraborty, A. D. Chien, K. D. Closser, V. Cofer-Shabica, S. Dasgupta, M. de Wergifosse, J. Deng, M. Diedenhofen, H. Do, S. Ehlert, P.-T. Fang, S. Fatehi, Q. Feng, T. Friedhoff, J. Gayvert, Q. Ge, G. Gidofalvi, M. Goldey, J. Gomes, C. E. González-Espinoza, S. Gulania, A. O. Gunina, M. W. D. Hanson-Heine, P. H. P. Harbach, A. Hauser, M. F. Herbst, M. Hernández Vera, M. Hodecker, Z. C. Holden, S. Houck, X. Huang, K. Hui, B. C. Huynh, M. Ivanov, Á. Jász, H. Ji, H. Jiang, B. Kaduk, S. Kähler, K. Khistyaev, J. Kim, G. Kis, P. Klunzinger, Z. Koczor-Benda, J. H. Koh, D. Kosenkov, L. Koulias, T. Kowalczyk, C. M. Krauter, K. Kue, A. Kunitsa, T. Kus, I. Ladjánszki, A. Landau, K. V. Lawler, D. Lefrancois, S. Lehtola, R. R. Li, Y.-P. Li, J. Liang, M. Liebenthal, H.-H. Lin, Y.-S. Lin, F. Liu, K.-Y. Liu, M. Loipersberger, A. Luenser, A. Manjanath, P. Manohar, E. Mansoor, S. F. Manzer, S.-P. Mao, A. V. Marenich, T. Markovich, S. Mason, S. A. Maurer, P. F. McLaughlin, M. F. S. J. Menger, J.-M. Mewes, S. A. Mewes, P. Morgante, J. W. Mullinax, K. J. Oosterbaan, G. Paran, A. C. Paul, S. K. Paul, F. Pavošević, Z. Pei, S. Prager, E. I. Proynov, Á. Rák, E. Ramos-Cordoba, B. Rana, A. E. Rask, A. Rettig, R. M. Richard, F. Rob, E. Rossomme, T. Scheele, M. Scheurer, M. Schneider, N. Sergueev, S. M. Sharada, W. Skomorowski, D. W. Small, C. J. Stein, Y.-C. Su, E. J. Sundstrom, Z. Tao, J. Thirman, G. J. Tornai, T. Tsuchimochi, N. M. Tubman, S. P. Veccham, O. Vydrov, J. Wenzel, J. Witte, A. Yamada, K. Yao, S. Yeganeh, S. R. Yost, A. Zech, I. Y. Zhang, X. Zhang, Y. Zhang, D. Zuev, A. Aspuru-Guzik, A. T. Bell, N. A. Besley, K. B. Bravaya, B. R. Brooks, D. Casanova, J.-D. Chai, S. Coriani, C. J. Cramer, G. Cserey, A. E. DePrince III, R. A. DiStasio, Jr., A. Dreuw, B. D. Dunietz, T. R. Furlani, W. A. Goddard III, S. Hammes-Schiffer, T. Head-Gordon, W. J. Hehre, C.-P. Hsu, T.-C. Jagau, Y. Jung, A. Klamt, J. Kong, D. S. Lambrecht, W. Liang, N. J. Mayhall, C. W. McCurdy, J. B. Neaton, C. Ochsenfeld, J. A. Parkhill, R. Peverati, V. A. Rassolov, Y. Shao, L. V. Slipchenko, T. Stauch, R. P. Steele, J. E. Subotnik, A. J. W. Thom, A. Tkatchenko, D. G. Truhlar, T. Van Voorhis, T. A. Wesolowski, K. B. Whaley, H. L. Woodcock III, P. M. Zimmerman, S. Faraji, P. M. W. Gill, M. Head-Gordon, J. M. Herbert, and A. I. Krylov, "Software for the frontiers of quantum chemistry: An overview of developments in the Q-Chem 5 package," J. Chem. Phys. **155**(8), 084801 (2021).
[45]A. D. McLean and G. S. Chandler, "Contracted Gaussian basis sets for molecular calculations. I. Second row atoms, $Z = 11–18$," J. Chem. Phys. **72**(10), 5639–5648 (1980).
[46]R. Krishnan, J. S. Binkley, R. Seeger, and J. A. Pople, "Self-consistent molecular orbital methods. XX. A basis set for correlated wave functions," J. Chem. Phys. **72**(1), 650–654 (1980).

[47]J. Wenzel, M. Wormit, and A. Dreuw, "Calculating core-level excitations and x-ray absorption spectra of medium-sized closed-shell molecules with the algebraic-diagrammatic construction scheme for the polarization propagator," J. Comput. Chem. **35**(26), 1900–1915 (2014).
[48]J. Wenzel, M. Wormit, and A. Dreuw, "Calculating X-ray absorption spectra of open-shell molecules with the unrestricted algebraic-diagrammatic construction scheme for the polarization propagator," J. Chem. Theory Comput. **10**(10), 4583–4598 (2014).
[49]E. Epifanovsky, K. Klein, S. Stopkowicz, J. Gauss, and A. I. Krylov, "Spin-orbit couplings within the equation-of-motion coupled-cluster framework: Theory, implementation, and benchmark calculations," J. Chem. Phys. **143**(6), 064102 (2015).
[50]C. Nicolas and C. Miron, "Lifetime broadening of core-excited and -ionized states," J. Electron Spectrosc. Relat. Phenom. **185**(8–9), 267–272 (2012).
[51]P. Wang, T. X. Carroll, T. D. Thomas, L. J. Sæthre, and K. J. Børve, "Calibration of oxygen 1s ionization energies. Accurate energies for CO_2, H_2O, CO, and O_2," J. Electron Spectrosc. Relat. Phenom. **251**, 147103 (2021).
[52]K. Siegbahn, *ESCA Applied to Free Molecules* (North-Holland Publishing Co., 1969).
[53]U. Gelius, "Binding energies and chemical shifts in ESCA," Phys. Scr. **9**(3), 133–147 (1974).
[54]S. G. Bratsch, "Revised Mulliken electronegativities: I. Calculation and conversion to Pauling units," J. Chem. Educ. **65**(1), 34 (1988).
[55]V. Feyer, O. Plekan, R. Richter, M. Coreno, G. Vall-llosera, K. C. Prince, A. B. Trofimov, I. L. Zaytseva, T. E. Moskovskaya, E. V. Gromov, and J. Schirmer, "Tautomerism in cytosine and uracil: An experimental and theoretical core level spectroscopic study," J. Phys. Chem. A **113**(19), 5736–5742 (2009).
[56]A. Kivimäki, J. Álvarez Ruiz, M. Coreno, M. Stankiewicz, G. Fronzoni, and P. Decleva, "Photoelectron spectroscopy of sulfur L levels in the SF_5CF_3 molecule," Chem. Phys. **353**(1–3), 202–208 (2008).
[57]M. A. Brisk and A. D. Baker, "Shake-up satellites in X-ray photoelectron spectroscopy," J. Electron Spectrosc. Relat. Phenom. **7**(3), 197–213 (1975).
[58]A. Föhlisch, P. Feulner, F. Hennies, A. Fink, D. Menzel, D. Sanchez-Portal, P. M. Echenique, and W. Wurth, "Direct observation of electron dynamics in the attosecond domain," Nature **436**(7049), 373–376 (2005).
[59]D. Toffoli, A. Guarnaccio, C. Grazioli, T. Zhang, F. Johansson, M. de Simone, M. Coreno, A. Santagata, M. D'Auria, C. Puglia, E. Bernes, M. Stener, and G. Fronzoni, "Electronic structure characterization of a thiophene benzo-annulated series of common building blocks for donor and acceptor compounds studied by gas phase photoelectron and photoabsorption synchrotron spectroscopies," J. Phys. Chem. A **122**(44), 8745–8761 (2018).
[60]E. Kukk, J. Niskanen, O. Travnikova, M. Berholts, K. Kooser, D. Peng, I. Ismail, M. N. Piancastelli, R. Püttner, U. Hergerhahn, and M. Simon, "Orientational anisotropy due to molecular field splitting in sulfur 2p photoemission from CS_2 and SF_6-theoretical treatment and application to photoelectron recoil," Phys. Chem. Chem. Phys. **26**(32), 21810–21820 (2024).
[61]O. Plekan, V. Feyer, R. Richter, M. Coreno, M. de Simone, K. C. Prince, A. B. Trofimov, E. V. Gromov, I. L. Zaytseva, and J. Schirmer, "A theoretical and experimental study of the near edge X-ray absorption fine structure (NEXAFS) and X-ray photoelectron spectra (XPS) of nucleobases: Thymine and adenine," Chem. Phys. **347**(1–3), 360–375 (2008).
[62]V. Feyer, O. Plekan, R. Richter, M. Coreno, M. de Simone, K. C. Prince, A. B. Trofimov, I. L. Zaytseva, and J. Schirmer, "Tautomerism in cytosine and uracil: A theoretical and experimental X-ray absorption and resonant Auger study," J. Phys. Chem. A **114**(37), 10270–10276 (2010).
[63]A. P. Hitchcock, J. A. Horsley, and J. Stöhr, "Inner shell excitation of thiophene and thiolane: Gas, solid, and monolayer states," J. Chem. Phys. **85**(9), 4835–4848 (1986).
[64]O. Baseggio, D. Toffoli, M. Stener, G. Fronzoni, M. de Simone, C. Grazioli, M. Coreno, A. Guarnaccio, A. Santagata, and M. D'Auria, "S2p core level spectroscopy of short chain oligothiophenes," J. Chem. Phys. **147**(24), 244301 (2017).
[65]R. L. Martin, "Natural transition orbitals," J. Chem. Phys. **118**(11), 4775–4777 (2003).